Available online at www.sciencedirect.com
ScienceDirect
International Journal of Heat and Fluid Flow 28 (2007) 871–881
International Journal of HEAT AND FLUID FLOW
www.elsevier.com/locate/ijhff

Lagrangian dispersion in turbulent channel flow and its relationship to Eulerian statistics

Jianping Luo [a], Tatsuo Ushijima [a,*], Osami Kitoh [a], Zhiming Lu [b], Yulu Liu [b]

[a] Nagoya Institute of Technology, Gokiso-cho, Showa-ku, Nagoya 466-8555, Japan
[b] Shanghai Institute of Applied Mathematics and Mechanics, Shanghai University, Shanghai 200072, China

Received 13 April 2006; received in revised form 21 November 2006; accepted 9 February 2007
Available online 19 April 2007

Abstract

Lagrangian and Eulerian statistics were obtained from the direct numerical simulation of a turbulent channel flow. The Eulerian integral time scales and time microscales were compared to their Lagrangian equivalents. It is found that the Lagrangian time scales equal the Eulerian time scales at the wall. Otherwise, these proved to be consistently larger than the Eulerian time scales, and the latter are also found to be scaled by the propagation velocity rather than the mean velocity. The near-wall behavior of the ratio of the Lagrangian to Eulerian integral time scales is explained by the difference between the mean velocity and the propagation velocity of the turbulent structure. The ratio is proportional to the inverse of the turbulence intensity ($T^{\mathrm{L}}/T^{\mathrm{E}} = \beta U/\sigma$). β for the streamwise component is nearly a constant value of 0.6 ($20 < y^+ < 70$), in agreement with atmospheric data and analyses. The ratio of the Lagrangian to the Eulerian time microscales is fairly constant away from the wall ($y^+ > 40$). After period over the integral time scale elapsed, the effect of shear on turbulent diffusion appears and the mean-square dispersion is almost proportional to t^3 in agreement with the predictions of Riley and Corrsin [The relation of turbulent diffusivities to Lagrangian velocity statistics for the simplest shear flow. J. Geophys. Res. 79 (1974) 1768–1771] for homogeneous shear flow. After particles are distributed fairly uniformly between two walls, the mean-square dispersion becomes proportional to t and in agreement with theory of Taylor's longitudinal dispersion.

Keywords: Turbulent channel flow; Lagrangian and Eulerian statistics; Turbulent diffusion

1. Introduction

Turbulent diffusion in a boundary layer is an important problem in predicting heat and mass transfer in both engineering and environmental flows (Legg and Raupach, 1982; Mazumder and Modest, 1997; Yeung and Pope, 1989). Turbulent diffusion is easier to understand physically within the Lagrangian framework (Taylor, 1921).

In this section, we first review some of the fundamental results concerning the turbulent diffusion of a fluid particle. Taylor (1921) devised the theory of turbulent dispersion. Let $X(x_0, t)$ denote the position at the time t of the fluid particle originating from x_0 at time $t = 0$ (for the 1-D case). For short diffusion times,

$$\langle X^2(x_0,t)\rangle \simeq \langle v'^2(x_0,t)\rangle t^2. \tag{1}$$

For long diffusion times,

$$\langle X^2(x_0,t)\rangle \simeq 2\langle v'^2(x_0,t)\rangle T^{\mathrm{L}} t, \tag{2}$$

where the Lagrangian integral time scale, T^{L}, is given by

$$T^{\mathrm{L}} = \int_0^\infty R^{\mathrm{L}}(\tau)\,\mathrm{d}\tau. \tag{3}$$

The coefficient $\langle v'^2\rangle T^{\mathrm{L}}$ in Eq. (2) is called the turbulent diffusivity, which holds that the turbulent diffusion is essentially Lagrangian (Tennekes and Lumley, 1972).

Corrsin (1953) extended Taylor's theory to a stationary homogeneous shear flow. Using the Taylor method, Corrsin

* Corresponding author.
E-mail address: ushijima@nitech.ac.jp (T. Ushijima).

0142-727X/$ - see front matter © 2007 Elsevier Inc. All rights reserved.
doi:10.1016/j.ijheatfluidflow.2007.02.008

Notation

L_{iix}	integral length scale of R_{ii}
Re_τ	Reynolds number based on half-channel width, $Re_\tau = u_\tau \delta / \nu$
R_{ii}	space–time correlation of u_i' velocity component
R_{ii}^{E}	Eulerian velocity autocorrelation
R_{ii}^{L}	Lagrangian velocity autocorrelation
t	time
T_i^{L}	Lagrangian integral time scale of v_i' velocity component
T_i^{E}	Eulerian integral time scale of u_i' velocity component
U	mean velocity in x direction
u_i'	Eulerian fluctuating velocity component in i direction
u_τ	friction velocity, $u_\tau = \sqrt{\tau_{\mathrm{w}}/\rho}$
v_i'	Lagrangian fluctuating velocity component in i direction
V_i	propagation velocity of turbulent structure of u_i' velocity component
X_i	displacement in i direction
x, y, z	streamwise, wall-normal and spanwise coordinates
Greek	
δ	half-channel width
ν	kinematic viscosity
ρ	density
λ_i	Taylor microscale of u_i' velocity component
τ	delay time
τ_i^{L}	Lagrangian time microscale of v_i' velocity component
τ_i^{E}	Eulerian time microscale of u_i' velocity component
τ_{w}	wall shear stress
Subscript and superscript	
0	initial reference point
$\langle\ \rangle$	ensemble average
$(\ )^+$	normalization by wall variables (u_τ, ν)

derived expression of the following form for the component of the streamwise dispersion

$$\begin{aligned}\langle X_1^2(x_0,t)\rangle = {} & S^2\langle v_2'^2(x_0,t)\rangle\left(\frac{2t^3}{3}\int_0^t R_{22}^{\mathrm{L}}(\tau)\,\mathrm{d}\tau\right. \\ & \left. -t^2\int_0^t \tau R_{22}^{\mathrm{L}}(\tau)\,\mathrm{d}\tau + \int_0^t \frac{\tau^3}{3}R_{22}^{\mathrm{L}}(\tau)\,\mathrm{d}\tau\right) \\ & + S\langle v_1'(x_0,t)v_2'(x_0,t)\rangle \\ & \times\left\{\int_0^t (t-\tau)^2\left[R_{12}^{\mathrm{L}}(\tau)+R_{21}^{\mathrm{L}}(\tau)\right]\mathrm{d}\tau\right. \\ & \left. + 2\int_0^t \tau(t-\tau)R_{12}^{\mathrm{L}}(\tau)\,\mathrm{d}\tau\right\} \\ & + 2\langle v_1'^2(x_0,t)\rangle\int_0^t (t-\tau)R_{11}^{\mathrm{L}}(\tau)\,\mathrm{d}\tau. \end{aligned} \tag{4}$$

For long diffusion times, this reduces to

$$\langle X_1^2(x_0,t)\rangle \simeq \frac{2}{3}\langle v_2'^2(x_0,t)\rangle S^2 T_2^{\mathrm{L}} t^3, \tag{5}$$

where S is the mean shear rate $\mathrm{d}U/\mathrm{d}y$. Eq. (5) shows that the effect of the mean velocity gradient greatly increases the dispersion over the isotropic case at long diffusion times.

Few data are available for Lagrangian properties because of the difficulty in conducting experimental measurements. Therefore, we need to infer the Lagrangian statistics from the Eulerian measurements, though little is known about the relationship between them. It has been suggested in theory (Pasquill and Smith, 1983) and from experiments on the atmospheric boundary layers (Hanna, 1981) that the ratio of Lagrangian to Eulerian integral time scales is proportional to the inverse of turbulent intensity ($T^{\mathrm{L}}/T^{\mathrm{E}} \propto U/\sigma$, where T^{E}, U and σ denote the Eulerian integral time scale measured at a fixed point, the mean velocity, and the rms fluctuation velocity, respectively). However, the suggested proportional constants are widely scattered. It has also been shown that the constant is dependent on the Reynolds number in a grid-generated turbulence (Sato and Yamamoto, 1987). It is not known whether these findings are applicable to strongly inhomogeneous flow fields where heat and mass transfer are important issues.

Direct numerical simulation is the best tool for investigating Lagrangian statistics, and some results have been reported for isotropic turbulence and homogeneous shear flows (Squires and Eaton, 1991). Although other results using the numerical simulation of a turbulent channel flow have also been reported (Kontomaris et al., 1992; Bernard and Rovelstad, 1994; Mito and Hanratty, 2002; Choi et al., 2004). They did not provide detailed Lagrangian statistics in the near-wall region. DNS may provide useful information for understanding the physical process of turbulent diffusion.

The aim of this study is to measure Lagrangian and Eulerian statistics and particle mean-square dispersions in a turbulent channel flow using DNS. The principal statistics are Lagrangian and Eulerian time scales (integral time scales and time microscales) that are envisaged to determine the characteristic velocity, length scale for these time scales in the near-wall region, and particle dispersions with time.

2. Numerical simulation

A direct numerical simulation of turbulent channel flow at a low Reynolds number was performed to evaluate the

velocities and trajectories of fluid particles. The Reynolds number Re_τ is 100; Reynolds number of the present simulation is at the lowest end of the turbulent channel flow. Near-wall coherent structure such as low-speed streak and quasi-streamwise vortex is yet realized in the simulation and we are particularly interested in the influence of the turbulence structure on the turbulent diffusion. Such influences will prevail even in a higher Reynolds number flow to a greater or lesser extent. The Reynolds number effects will be discussed later by comparing with the results from other researchers.

The pseudo-spectral numerical scheme was used in this study. The domain size in the streamwise, wall-normal, and spanwise directions is $1880 \times 200 \times 630$ in wall units, respectively. The corresponding grid number in each direction is $96 \times 65 \times 64$. The resolution in the streamwise and spanwise directions were $\Delta x^+ = 19.6$, $\Delta z^+ = 9.8$. The grid resolution is comparable to the one used by Iida and Nagano (1998), which fully resolved the essential turbulent scales. The velocity fields were computed and stored at the interval $\Delta t^+ = 0.2$ for a period of 3000 in wall units. Two consecutive velocity fields were used to track the particles for each time step. The first-order Euler's scheme was used twice in sequence (known as the predictor–corrector scheme) for the initial step, and the second-order Adams–Bashforth scheme was used to compute the particle trajectories for the remaining time steps (Kontomaris et al., 1992). 4096 particles were released from each plane at a specified wall-normal location. A quarter of these particles are released four times at $\Delta t^+ = 100$ interval. Half of these particles were released from the flow in the lower half of the channel and the other half in the upper half. Each set of particles (512 particles) were uniformly distributed and released at each plane. Using these particles, Lagrangian statistics were computed. Since the instantaneous position of a particle does not, in general, coincide with a grid point, the particle velocity has to be evaluated by a three-dimensional interpolation of the Eulerian velocity grid-point data (Kontomaris et al., 1992). Fluid particle velocity along a particle trajectory was computed by employing third order Hermite polynomials in the homogeneous directions and a Chebyshev polynomial in the wall-normal direction (Ushijima et al., 2003). Periodic boundary conditions were imposed on the streamwise and spanwise directions to obtain the velocity of the fluid particles. In the present paper, the subscripts $i = 1$, 2 and 3 denote the streamwise, wall-normal and spanwise components, respectively.

3. Lagrangian statistics

Lagrangian velocity autocorrelations $R^{\mathrm{L}}_{ii}(\tau; y)$ shown in Fig. 1 are defined (Mito and Hanratty, 2002) as

$$R^{\mathrm{L}}_{ii}(\tau; y) = \frac{\left\langle \frac{v_i'(t,y)}{\sigma_i^0} \frac{v_i'(t+\tau,y)}{\sigma_i^\tau} \right\rangle}{\left\langle \left(\frac{v_i'(t,y)}{\sigma_i^0} \right)^2 \right\rangle^{1/2} \left\langle \left(\frac{v_i'(t+\tau,y)}{\sigma_i^\tau} \right)^2 \right\rangle^{1/2}}, \tag{6}$$

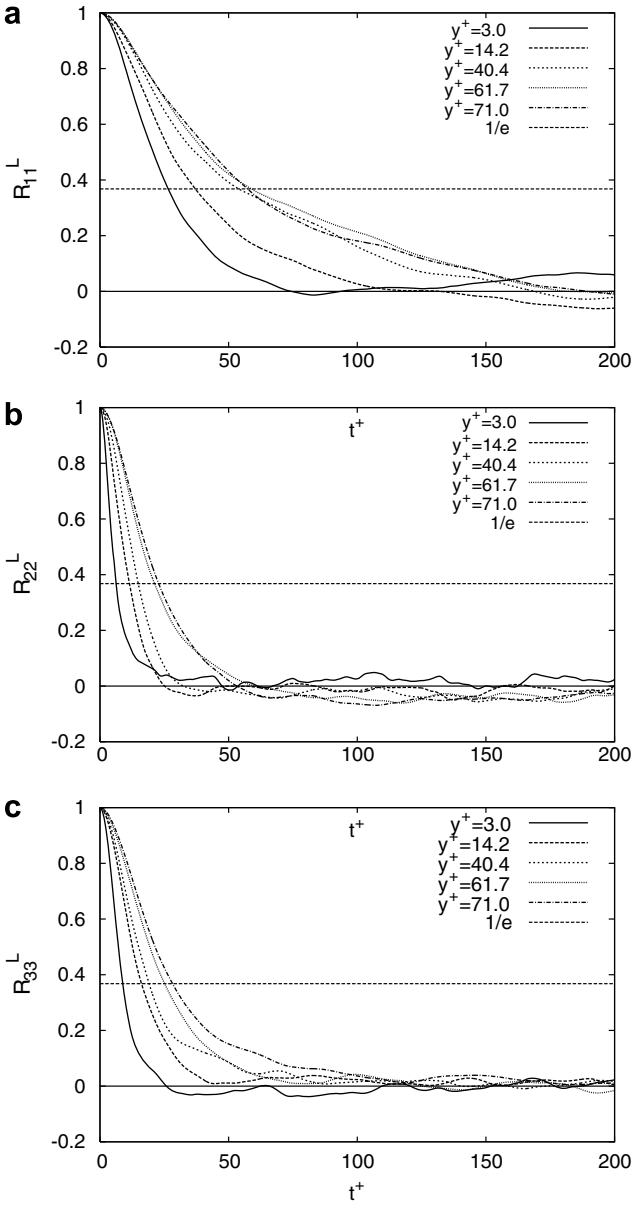

Fig. 1. Lagrangian velocity autocorrelations for particles at $y^+ = 3.0$, 14.2, 40.4, 61.7 and 71.0 in streamwise (a), wall-normal (b) and spanwise directions (c).

where $v_i'(t+\tau, y)$ is the Lagrangian fluctuation velocity starting at time t and position y, σ_i is the Eulerian root-mean square of the velocity fluctuations in the i-direction ($\sigma_i^0 = \langle u_i'^2(y) \rangle^{1/2}$, $\sigma_i^\tau = \sigma_i(y'(\tau,y)), y'(\tau,y) = \int_0^\tau v_2'(t,y)\,\mathrm{d}t + y$), and the angle bracket $\langle\ \rangle$ denotes the ensemble average, with no summation convention applied to repeated indices. It is clear from this figure that the autocorrelations in the streamwise direction decrease less rapidly than those in the other directions for all initial particle locations, and that they decrease more rapidly for particles initially located in the viscous sublayer than those in the buffer layer and logarithmic region. This observation agrees well with that in Deardorff and Peskin (1970), and a similar behavior of the autocorrelations was also observed by Wang et al.

(1995), who carried out large eddy simulations of a fully developed turbulent channel flow.

The Lagrangian integral time scale T_i^{L} for i-velocity component can be obtained from R_{ii}^{L} profile as

$$T_i^{\mathrm{L}} = \int_0^{\infty} R_{ii}^{\mathrm{L}}(\tau)\,\mathrm{d}\tau. \tag{7}$$

As a simple method, it is convenient to estimate T_i^{L} as a time needed for the R_{ii}^{L} to decrease to $1/e$. Mito and Hanratty (2002) have reported that the Lagrangian integral time scale defined as the time at which $R_{ii}^{\mathrm{L}} = 1/e$ almost coincides with the time scale obtained from the integral of R_{ii}^{L}. Fig. 2 shows the comparison between the Lagrangian integral time scale defined by Eq. (7) and that from simple method. Here, the integral range is limited to a finite value of t_Z, the first zero-cross time of $R_{ii}^{\mathrm{L}}(\tau)$, instead of adopting the infinite time. Both values almost coincide with each other for every components. Thus, all integral time scales in this paper were estimated according to the simple method.

Fig. 3 shows the distribution of a Lagrangian integral time scale $T_i^{\mathrm{L}+}$ versus the coordinate y^+ (a) and y/δ (b). In the figure, we also plotted the results of Mito and Hanratty (2002, quoted as MH in the figure). Their results are for $Re_\tau = 150$ and 300. The trend of their results approaching the wall ($y^+ < 10$) is the same as ours. Approaching the wall, the time scales decrease but seem to approach a non-zero value at the wall ($T_1^{\mathrm{L}+} = 21$, $T_2^{\mathrm{L}+} = 4$, $T_3^{\mathrm{L}+} = 6$). $T_2^{\mathrm{L}+}$ and $T_3^{\mathrm{L}+}$ agree well with the results of Mito and Hanratty in the whole region. In the streamwise component, $T_1^{\mathrm{L}+}$ agrees with each other at $y^+ \leqslant 10$, but the present result is greater than that of Mito and Hanratty in the intermediate layer ($10 < y^+ < 70$). The difference of the results may be due to the Reynolds number variation. The time scales are constant in the center region ($y^+ \geqslant 70$), while those of Mito and Hanratty increase monotonically. If y is scaled by δ, the results of Mito and Hanratty for $Re_\tau = 300$ show the constant region in the channel center region ($y/\delta \geqslant 0.7$). This trend in the center region is plausible since the turbulence in these region is almost homogeneous. The result of Wang et al. ($Re_\tau = 180$) is also compared well with the present ones. Therefore, the present result is equally valid with the previous researcher's. Fig. 3b also shows dependence of $T_1^{\mathrm{L}+}$ on the Reynolds number, $T_1^{\mathrm{L}+}$ increases with the Reynolds number in the core region.

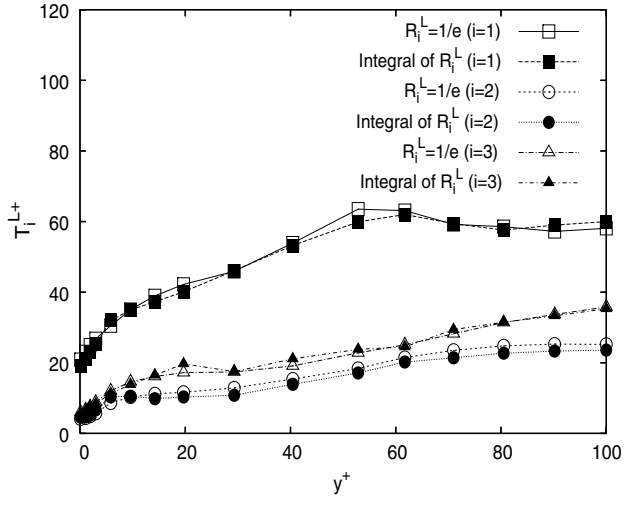

Fig. 2. Comparison of the Lagrangian integral time scale defined as the time at which $R_i^{\mathrm{L}} = 1/e = 0.368$ and the Lagrangian integral scale.

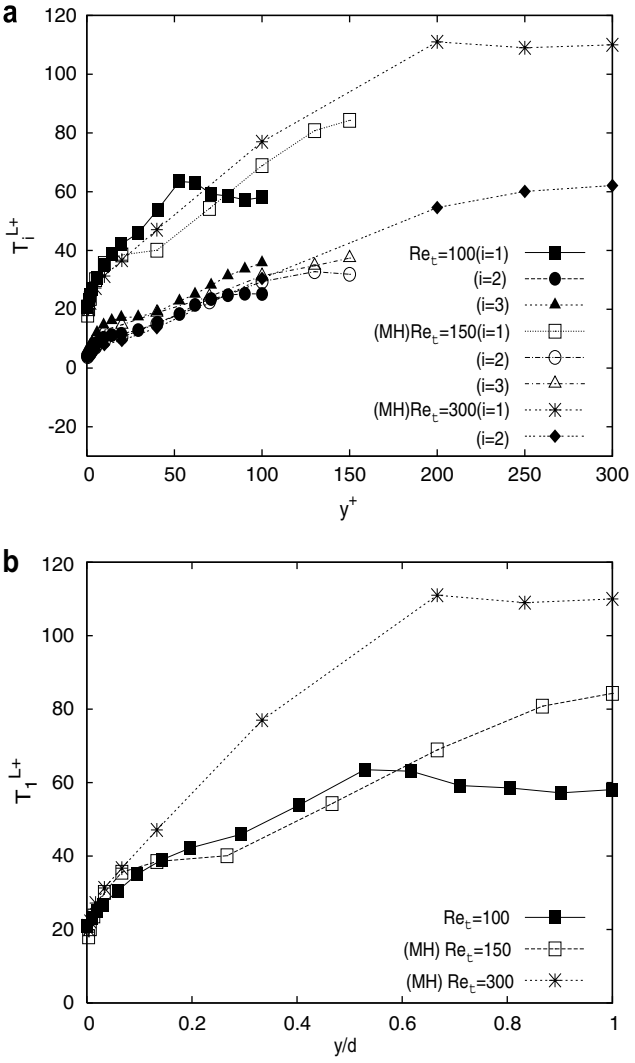

Fig. 3. Comparison of Lagrangian integral time scales versus the coordinate y^+ (a), and y/δ (b).

It is found that the time scales in the buffer layer ($10 \leqslant y^+ \leqslant 30$) are nearly constant. In the buffer layer, there exists a quasi-streamwise turbulent structure, such as a streamwise vortex and high- and low-speed streaks. The velocity field there is fairly two dimensional and the streamwise vortex plays a role of transporting momentum. The diameter of the streamwise vortex is almost the same as the thickness of the buffer layer. Therefore, the time scale of the cross component are characterized by the thickness of the buffer layer and the characteristic velocity of the streamwise vortex in the buffer layer. The streamwise velocity is advected by the streamwise vortex to often form the streaks. The streaks are much longer structure in the

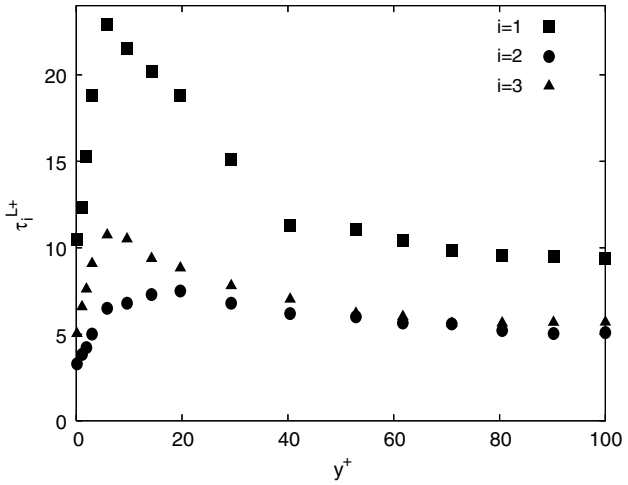

Fig. 4. Comparison of Lagrangian time microscales.

streamwise direction than the streamwise vortex. This fact explains why the time scale in the streamwise velocity is greater than the others. This can be also inferred from the spatial correlation in the streamwise direction where the streamwise velocity correlation is greater than the cross component velocity correlations.

Now, we turn attention to the time microscales, which are associated with a small-scale eddy. The Eulerian and Lagrangian time microscales are defined as

$$\frac{1}{(\tau_i^{\mathrm{E}})^2} = \frac{1}{2\sigma_i^2}\left[\left\langle\left(\frac{\partial u_i'}{\partial t}\right)^2\right\rangle\right]_{t=0} = -\frac{1}{2}\left[\frac{\partial^2 R_{ii}^{\mathrm{E}}}{\partial t^2}\right]_{t=0}, \tag{8}$$

$$\frac{1}{(\tau_i^{\mathrm{L}})^2} = \frac{1}{2\sigma_i^2}\left[\left\langle\left(\frac{\partial v_i'}{\partial t}\right)^2\right\rangle\right]_{t=0} = -\frac{1}{2}\left[\frac{\partial^2 R_{ii}^{\mathrm{L}}}{\partial t^2}\right]_{t=0}, \tag{9}$$

where u_i' is the Eulerian fluctuation velocity.

In this study, τ_i^{E} and τ_i^{L} are evaluated by using the first half of Eqs. (8) and (9), namely, the mean square of the first derivative of the velocity. The first derivative is evaluated by a central difference approximation. These values are also evaluated by using the second derivative of the correlation. The values evaluated by both methods agree to each other within 1% difference. Lagrangian time microscales $\tau_i^{\mathrm{L}+}$ are shown in Fig. 4. It is clear from the figure that the Lagrangian time microscale of the streamwise direction is larger than that of the others, especially near the wall. $\tau_i^{\mathrm{L}+}(i=2$ and $3)$ vary similarly away from the wall $(y^+ > 30)$. $\tau_i^{\mathrm{L}+}$ near the wall has a non-zero value that rises steeply (up to $y^+ = 10$). Fig. 4 shows that the Lagrangian time microscales for the three directions are fairly constant away from the wall $(y^+ > 40)$.

4. Eulerian statistics

The Eulerian velocity autocorrelations $R_{ii}^{\mathrm{E}}(\tau; y)$ shown in Fig. 5 are defined as

$$R_{ii}^{\mathrm{E}}(\tau; y) = \frac{\langle u_i'(t, y) u_i'(t+\tau, y)\rangle}{\langle u_i'^2(y)\rangle}. \tag{10}$$

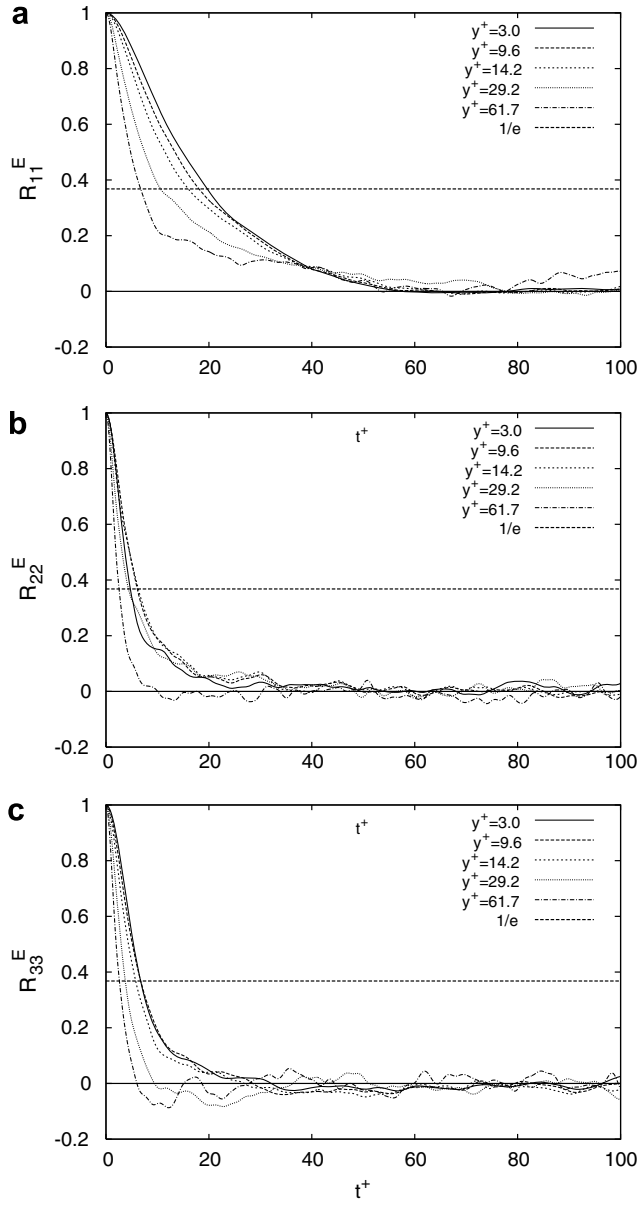

Fig. 5. Eulerian velocity autocorrelations for particles at $y^+ = 3.0$, 9.6, 14.2, 29.2 and 61.7 in streamwise (a), wall-normal (b) and spanwise directions (c).

It is clear from this figure that the Eulerian velocity autocorrelations in the streamwise direction decrease less rapidly than those in the other directions, and that the autocorrelations decrease with distance from the wall.

The Eulerian integral time scale obtained from Eulerian velocity autocorrelations is presented in Fig. 6. In the figure, the results of Wang et al. (1995) and Nishimura (2000) are also compared. T_1^{E+} agrees well with the experimental result (Nishimura) and LES result (Wang et al.).

It might be thought that the Eulerian time scale is controlled by the advection of the turbulent structure. In the near-wall region, it is not valid to apply Taylor's frozen turbulence hypothesis using the local mean velocity. In order to discover the appropriate velocity scale, we first

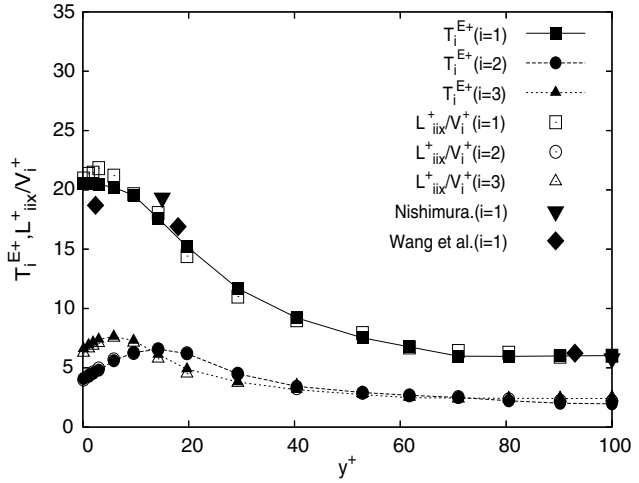

Fig. 6. Eulerian integral time scales and the time scale defined by the integral length scale in the streamwise direction (L_{iix}) and the propagation velocity (V_i). Wang et al. (1995) ($Re_\tau = 180$). Nishimura (2000) ($Re_\tau = 100$).

evaluated the propagation velocity of the turbulent structure, relating u_i' velocity component by

$$V_i = \frac{\Delta x_{\max}}{\Delta t}, \tag{11}$$

where $\Delta x_{\max}$ is a peak location in the space–time correlation,

$$R_{ii}(\Delta x, y, \Delta t) = \frac{\langle u_i'(x,y,t)u_i'(x+\Delta x, y, t+\Delta t)\rangle}{\langle u_i'^2(y)\rangle}. \tag{12}$$

No summation convention was applied, and $\Delta t^+ = 18$ was adopted in the present study. Kim and Hussain (1993) evaluated the propagation velocity from their DNS data. They varied Δt^+ from 3 to 27 and found that there was no difference in choosing Δt^+ (for details see Kim and Hussain, 1993) for V_i evaluation. The propagation velocity V_i^+ shown in Fig. 7 is faster than the local mean velocity near the wall. V_2^+ and V_3^+ are slightly faster than V_1^+. Schoppa and Hussain (2000) showed from their DNS data that the low speed streak was formed and trailed by streamwise vortices and it resulted in the former being longer than the latter. The difference among the propagation velocities reflects this fact. There are intersecting points between the profiles of the local mean and propagation velocity in the buffer layer. The propagation of the turbulent velocity structure lags slightly behind the mean velocity at the center of the channel. This suggests that the turbulence structures, contributing to the average propagation velocity move away from the wall resulting in the propagation velocity being lower than the local average (Kim and Hussain, 1993).

It was found that the turbulent structure propagates downstream like a wave. It was, therefore, natural to consider that the Eulerian time scale is characterized by the integral length scale and the propagation velocity. To examine the time scale, we evaluated the integral length scale in the streamwise direction using R_{ii}.

The integral length scale L_{iix} plotted in the streamwise direction in Fig. 8 is defined as

$$L_{iix}(y) = \int_0^\infty R_{ii}(x,y,0)\,\mathrm{d}x. \tag{13}$$

The streamwise component L_{iix} is quite large near the wall compared with the other components. The time scale defined as a ratio of the integral length scale in the streamwise direction (L_{iix}) to the propagation velocity (V_i) is plotted in Fig. 6 together with the Eulerian integral time scale T_i^{E}. It is clearly seen from this comparison that both time scales agree very well with each other.

Fig. 9 shows the distribution of Eulerian time microscales τ_i^{E} measured at a fixed point, and that of the time microscale defined by the Taylor microscale (λ_i) and the propagation velocity (V_i). The Taylor microscale (λ_i) is defined as

$$\frac{1}{(\lambda_i)^2} = \frac{1}{\sigma_i^2}\left[\left\langle\left(\frac{\partial u_i'}{\partial x}\right)^2\right\rangle\right]_{x=0} = -\frac{1}{2}\left[\frac{\partial^2 R_{ii}}{\partial x^2}\right]_{x=0}, \tag{14}$$

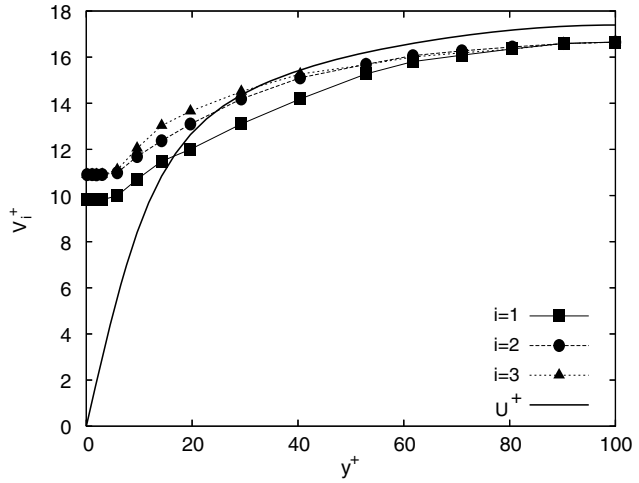

Fig. 7. Propagation velocity.

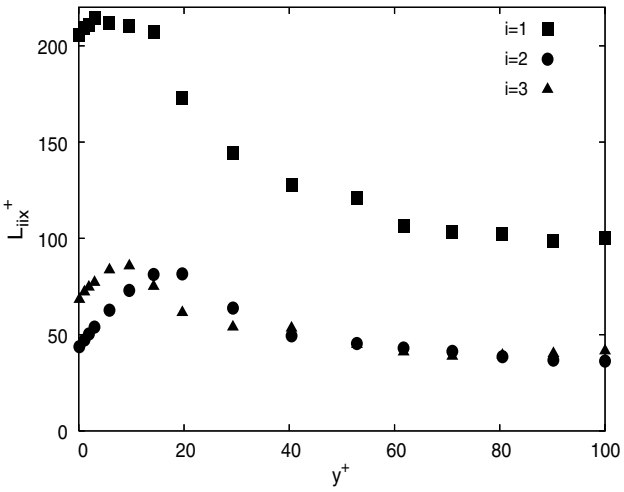

Fig. 8. Comparison of integral length scales.

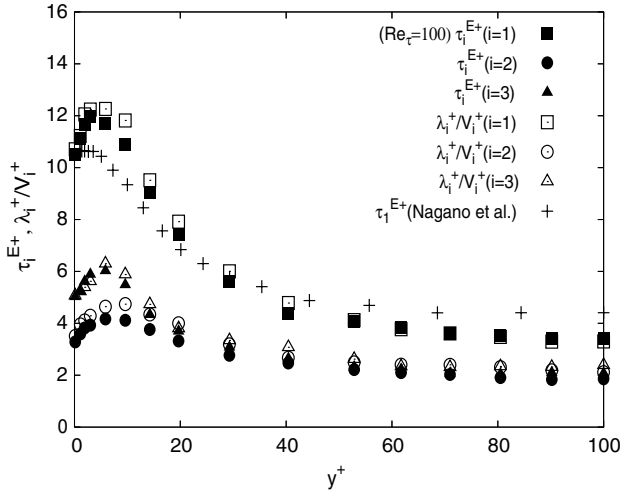

Fig. 9. Fixed Eulerian time microscales and time microscale defined by Taylor microscale (λ_i) and the propagation velocity (V_i). Nagano et al. (1998) ($Re_\tau = 800$) based on boundary layer thickness.

where R_{ii} is the space correlation. In the figure, τ_1^{E} measured by Nagano et al. (1998) is also plotted. The experimental result almost coincides with that from DNS. From Figs. 6 and 9, the Eulerian integral and time microscales are expressed using the propagation velocity of the turbulent structure and the appropriate length scales like

$$T_i^{\mathrm{E}} \approx \frac{L_{iix}}{V_i}, \tau_i^{\mathrm{E}} \approx \frac{\lambda_i}{V_i}. \tag{15}$$

5. Relationship between Lagrangian and Eulerian time scales

It is easy to experimentally measure the Eulerian integral time scale and the Taylor microscale. It is therefore very useful to relate the Lagrangian to the Eulerian time scales in order to estimate turbulent diffusion.

Fig. 10 depicts the ratio of Lagrangian to Eulerian integral time scales against y^+. This figure shows that the Lagrangian and Eulerian integral time scales are equal at the wall. This is because the mean velocity close to the wall is almost zero, and the displacement of fluid particles is so small that the position of the particles is not different from that of the fixed measuring point (Iliopoulos and Hanratty, 1999). The ratio linearly increases with the distance from the wall until $y^+ = 10$ for all components. Time scales are determined by transit time of the same turbulent structure seen by a fixed Eulerian observer and a wandering Lagrangian observer. The passing speed of the turbulence structure seen by a fixed Eulerian observer and a wandering Lagrangian observer is different, while the characteristic length scale in the vicinity of the wall is shared by both observers, who see the same turbulence structure. The turbulent structure passes the fluid particles at the speed of $V_i - U$. In Fig. 7, $U^+ = y^+$ and $V_i^+ = 10 \sim 12$ near the wall ($y^+ < 10$). Consequently, the ratio can be expressed by

$$\frac{T_i^{\mathrm{L}}}{T_i^{\mathrm{E}}} = \frac{V_i}{V_i - U} = \left(1 - \frac{U}{V_i}\right)^{-1} \approx \left(1 + \frac{U}{V_i}\right) = 1 + \frac{y^+}{10}. \tag{16}$$

Eq. (16) is shown by the solid line in Fig. 10. Physical interpretation of Eq. (16) is that the difference between the time scales close to the wall is determined by the difference of passing speeds of the turbulence structure viewed by Lagrangian and Eulerian observers. Strictly speaking, Eq. (16) is only valid very close to the wall ($y^+ < 10$) and it becomes indeed invalid where $V_i \sim U$. To improve the equation, the effect of fluid mixing by the turbulence structure should be taken into account. From Fig. 10, however, trend of the linear increase seems to extend to the region farther away from the wall. In the region away from the wall ($y^+ > 40$), the Lagrangian integral time scale is known to vary in proportion to the distance from the wall (Deardorff and Peskin, 1970). Fig. 6 shows that the Eulerian integral time scale is fairly constant there, which explains the linear increase of the ratio. On the other hand, the ratio is constant for the wall-normal component in the buffer layer ($5 < y^+ < 20$), and then increases linearly. In Fig. 10, the LES results from Wang et al. (1995) are also compared. Except for $i = 2$ and 3 at $y^+ \approx 90$, the results almost coincide with ours.

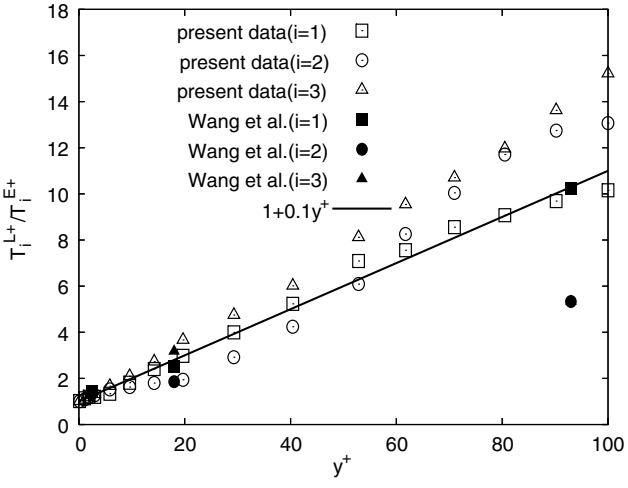

Fig. 10. Ratio of Lagrangian to Eulerian integral time scales in wall coordinate. Wang et al. (1995) ($Re_\tau = 180$).

The ratio of the Lagragian integral time scale to the Eulerian one is reportedly proportional to the turbulent intensity, i.e., $T_i^{\mathrm{L}}/T_i^{\mathrm{E}} = \beta U/\sigma_i$, ($\beta =$ constant). Many researchers tried to determine the proportional constant both experimentally and theoretically. However, the suggested constant ranges from 0.35 to 0.8 (Koeltzsch, 1999). Philip (1967) used an assumed space–time correlation to evaluate the proportional constant. His result, however, suggests that the proportional constant is not really constant but depends on the space–time correlation. Sato and Yamamoto (1987) estimated the proportional constant experimentally in a grid-generated turbulence and found that the value decreases with an increase in the Reynolds number.

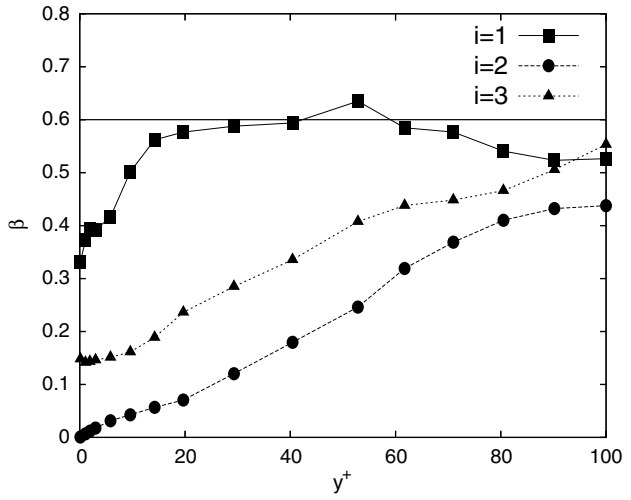

Fig. 11. Variation of β in three directions.

Fig. 11 shows the value of β in three directions. For the streamwise component, $\beta \approx 0.3$ at the wall and increases to 0.6 up to $y^+ \approx 20$. In the range of $20 < y^+ < 70$, β takes a nearly constant value of 0.6, followed by some decrease of β at the center region. For the wall-normal component, β increases monotonically with y^+ from zero value at the wall. The value of the spanwise component varies in a range between those of the streamwise and the wall-normal components. Wang et al. (1995) utilized a large eddy simulation to obtain Lagrangian statistics at three different heights (one each for a viscous sublayer, a buffer layer, and a logarithmic layer) and suggested a value of 0.6 (in their paper, the timescale T^{L} and T^{E} have been averaged over the three components).

Fig. 12 shows the ratio of Lagrangian to Eulerian time microscales along the wall-normal direction. The Lagrangian and Eulerian time microscales are equal at the wall. The ratio increases linearly at a short distance from the wall, and then approaches a constant asymptotically. The empirical formula showing the variation is given as

$$\frac{\tau_i^{\mathrm{L}}}{\tau_i^{\mathrm{E}}} \approx 2.75 - 1.75 \exp\left(-\frac{y^+}{16}\right). \tag{17}$$

This expression is shown in Fig. 12. The ratio assumes a constant value of 2.75 at the center of the channel. Shlien and Corrsin (1974) experimentally obtained Lagrangian statistics by heat dispersion behind a heated line source in grid-generated turbulence in a wind tunnel. Compared to the Eulerian results obtained from the same facility (Comte-Bellot and Corrsin, 1971), $\tau^{\mathrm{L}}/(\lambda/V)$ (i.e. $\tau^{\mathrm{L}}/\tau^{\mathrm{E}}$) is about 2, and is in the same order as our results obtained.

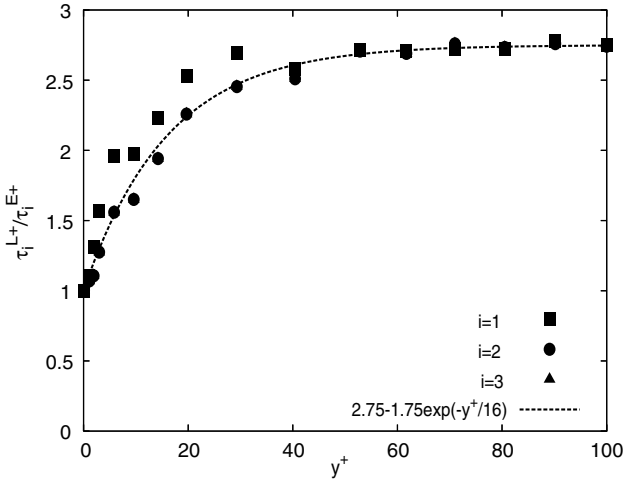

Fig. 12. Ratio of Lagrangian to Eulerian time microscales in wall coordinate.

6. Particle dispersion

In this study, the mean-square dispersion $\langle X_i^2 \rangle$ was calculated from

$$\langle X_i^2 \rangle(t, y_0) = \langle [X_i(t_0 + t) - X_i(t_0) - \langle X_i(t_0 + t) - X_i(t_0) \rangle]^2 \rangle. \tag{18}$$

To study dispersion, the average of the displacement is subtracted in this study.

The mean-square dispersion $\langle X_i^2 \rangle$ in three directions for particles released from the viscous sublayer ($y^+ = 3.0$), buffer layer ($y^+ = 19.7$), log layer ($y^+ = 52.9$) and central region ($y^+ = 90.2$) is shown in Fig. 13. The results of $\langle X_1^2 \rangle$ show that particles released from each layer disperse in proportion to t^2 for short diffusion times. Around $t^+ = T_1^{\mathrm{L}+}$, which varies from 27 to 57 for the particles released from different layers, the power index of t is reduced to less than 2, indicating the transition of the power index from 2 to 1 according to Taylor's theory. After a period of the integral time has elapsed, the mean-square dispersion increases in proportion to t^n ($n > 2$). This is because mean shear starts to have an effect on the turbulent diffusion. Except for particles released from the viscous sublayer, when the effect of shear turns in, the power index increases to 3 that is the same as given in the theory of turbulent diffusion in a homogeneous shear flow (Riley and Corrsin, 1974). For particles released from viscous sublayer, the power index n is larger than 3. For even longer times, after the particles disperse uniformly between two walls, the dispersion becomes proportional to t, in accordance to Taylor's longitudinal theory (Taylor, 1953). Wang et al. (1995), using LES, also reported that the dispersion is proportional to t for sufficiently long times.

Following the theory of Riley and Corrsin (1974), the dispersion time scale T_1^* at which the effect of mean shear appears can be estimated as follows. Assume that $R_{11}^{\mathrm{L}}(\tau) = \exp(-\tau/T_1^{\mathrm{L}}), R_{22}^{\mathrm{L}}(\tau) = \exp(-\tau/T_2^{\mathrm{L}})$ and $R_{12}^{\mathrm{L}}(\tau) = R_{21}^{\mathrm{L}}(\tau) = \exp(-\tau/T_{12}^{\mathrm{L}})$, where T_{12}^{L} is the Lagrangian integral time scale for $R_{12}^{\mathrm{L}}(\tau)$, the mean-square dispersion in the streamwise direction for a homogeneous shear flow becomes

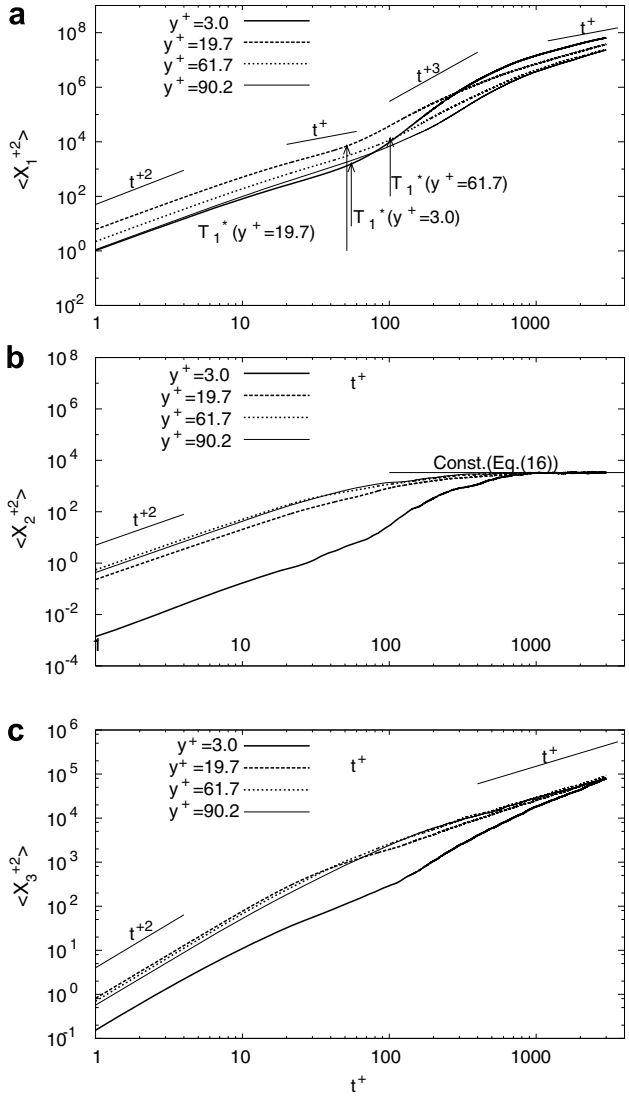

Fig. 13. Mean-square dispersion in the streamwise (a), wall-normal (b) and spanwise directions (c). Particles released from the viscous sublayer, buffer layer, log layer and central region.

$$\frac{\langle X_1^2(t)\rangle}{\langle v_1'^2\rangle (T_1^{\mathrm{L}})^2} = 2\left(\frac{t}{T_1^{\mathrm{L}}} - \left(1-\mathrm{e}^{-t/T_1^{\mathrm{L}}}\right)\right) + \frac{\langle v_2'^2\rangle (T_2^{\mathrm{L}})^2}{\langle v_1'^2\rangle (T_1^{\mathrm{L}})^2} S^2 (T_2^{\mathrm{L}})^2 \times \left\{ \frac{2}{3}\left(\frac{t}{T_2^{\mathrm{L}}}\right)^3 - \left(\frac{t}{T_2^{\mathrm{L}}}\right)^2 - 2\left(\frac{t}{T_2^{\mathrm{L}}}\right)\mathrm{e}^{-t/T_2^{\mathrm{L}}} + 2\left(1-\mathrm{e}^{-t/T_2^{\mathrm{L}}}\right)\right\} + \frac{S\langle v_1' v_2'\rangle (T_{12}^{\mathrm{L}})^3}{\langle v_1'^2\rangle (T_1^{\mathrm{L}})^2} \times \left\{ \left(\frac{t}{T_{12}^{\mathrm{L}}}\right)^2 - \left(\frac{t}{T_{12}^{\mathrm{L}}}\right)\left(1-\mathrm{e}^{-t/T_{12}^{\mathrm{L}}}\right)\right\}. \quad (19)$$

In the present study, the cross-correlation R_{12}^{L} was not computed. From the results obtained from Wang et al. (1995), $T_{12}^{\mathrm{L}} \lessapprox T_2^{\mathrm{L}}$. In Eq. (19), the term including $\langle v_1' v_2'\rangle$ is proportional to t^3 and is smaller than the first term that is proportional to t^2 for short times with respect to the integral time scale. For very long times, the term including S^2 is proportional to t^3 and the term of $\langle v_1' v_2'\rangle$ is proportional to t^2. Therefore, the effect of $\langle v_1' v_2'\rangle$ on the dispersion is secondary for both short and long diffusion times. In order to estimate the time for shear effect to appear (T_1^*), only the term of S^2 needs to be considered and T_1^* is given by

$$T_1^* = \left(\frac{3}{2}\frac{T_1^{\mathrm{L}}}{S^2}\frac{\langle v_1'^2\rangle T_1^{\mathrm{L}}}{\langle v_2'^2\rangle T_2^{\mathrm{L}}}\right)^{\frac{1}{3}}. \quad (20)$$

which is the inverse of the cubic root of the coefficient in the t^3 term of Eq. (19). The effect of shear starts to appear, when t elapsed over the period of T_1^*. T_1^* becomes smaller, as either the shear rate (S) or the wall-normal dispersion rate ($\langle v_2'^2\rangle T_2^{\mathrm{L}}$) has a larger quantity. When neither shear nor wall-normal dispersion exists, T_1^* is infinity, and no shear-effect comes out. Comparing the term of t^3 with the first term, the mean-square dispersion is proportional to t^2 for short diffusion times, then becomes proportional to t^1, and finally to t^3 under the influence of shear when $T_1^* \gg T_1^{\mathrm{L}}$. In Fig. 13a, T_1^* for each case is indicated by an arrow. The dispersion rate increases significantly when t exceeds beyond T_1^* due to the shear effect. Except for $y^+ = 3.0$ (viscous sublayer) case, the power index n approaches 3 in accordance to the theory of Riley and Corrsin for homogeneous shear flow. For $y^+ = 3.0$ case, the power index n is larger than 3. The large power index for $y^+ = 3.0$ case is due to the large inhomogeneity in turbulent flow fields, in which the particles have to pass through during the diffusing process. Present result indicates that Riley and Corrsin's theory can be applicable even for channel flow except for viscous sublayer where the large inhomogeneity prevails.

The computed T_1^* is depicted in Fig. 13a, which shows that after T_1^*, the mean-square dispersion increases more rapidly due to the influence of shear. It also shows that Eq. (20) can reasonably predict the timing for the shear-effect to appear in the mean-square dispersion.

The mean-square dispersion $\langle X_2^2\rangle$ is proportional to t^2 for short diffusion times, and becomes constant. For sufficiently long diffusion times, since due to the wall constraint the particles dispersed uniformly between the two walls. Therefore, the mean-square dispersion can be evaluated by

$$\langle X_2^2(t\to\infty)\rangle = \frac{\int_{-\delta}^{\delta} y^2\,\mathrm{d}y}{\int_{-\delta}^{\delta}\mathrm{d}y} = \frac{\delta^2}{3}. \quad (21)$$

This value is also shown in Fig. 13b. The mean-square dispersion of the particles approaches the estimated value. If Re_τ increases, it is reasonably inferred that the period of dispersion proportional to t^1 would appear before approaching the asymptotic value (Wang et al., 1995). The mean-square dispersion of particles released from the viscous sublayer increases in proportion to t^2, even after the time over the integral time scale has elapsed ($T_2^{\mathrm{L}+} = 6.3$, at $y^+ = 3.0$). At $t^+ \approx 50$, the power index exceeds 2. This is because the turbulent velocity increases rapidly during particle motion away from the wall. Most of the particles released from the viscous sublayer remain in the viscous sublayer until $t^+ \approx 100$.

Apart from the particles released from the viscous sublayer, the mean-square dispersion $\langle X_3^2 \rangle$ is proportional to t^2 for short diffusion times, and to t^1 for long diffusion times. In the spanwise direction, there are no constraints such as the wall and the effect of shear, and the spanwise rms velocity remains almost constant. Therefore, Taylor's diffusion theory becomes applicable without modification. For the particles released from the viscous sublayer, the dispersion is proportional to t^2 for short times, after which the power index of t decreases to slightly less than 2 for a while, and then becomes at about 2, and finally the dispersion becomes proportional to t^1. The reason why the dispersion increases for intermediate period between the first stage ($\propto t^2$) and the final stage ($\propto t^1$) is probably due to the rms velocity profile near the wall.

7. Conclusion

Lagrangian and Eulerian statistics in a turbulent channel flow of $Re_\tau = 100$ are evaluated using DNS. The relationship between two statistics and the behavior of particle dispersion are discussed in relation to the results reported for homogeneous or homogeneous shear flows. The main conclusions obtained are summarized as follows.

The Lagrangian integral time scales T_i^{L} are equal to the Eulerian integral time scales T_i^{E} at the wall and have non-zero values there. $T_1^{\mathrm{L}+}$ (streamwise component) increases from 20 at the wall with y^+ and takes a nearly constant value of 60 in the channel center region ($y^+/\delta \geqslant 0.7$).

The Eulerian integral time scale can be approximated by the ratio of the integral length scale in the streamwise direction to the propagation velocity of the turbulence structure, i.e., it is determined by the propagation of the turbulence structure.

The ratio of Lagrangian to Eulerian integral time scales $T_i^{\mathrm{L}}/T_i^{\mathrm{E}}$ is given by Eq. (16) for $y^+ \leqslant 10$. For streamwise and spanwise component ($i = 1$ and 3), $T_i^{\mathrm{L}}/T_i^{\mathrm{E}}$ increases almost linearly with y^+ over the whole channel while for wall-normal component it takes a constant in the buffer layer and increase linearly for $y^+ \geqslant 20$. β, another measure of the ratio between two integral time scales defined as $T_i^{\mathrm{L}}/T_i^{\mathrm{E}} = \beta(U/\sigma_i)$, has nearly constant value of 0.6 for $i = 1$ in the range of $20 \leqslant y^+ \leqslant 70$. For $i = 2$ and 3, β increases monotonically with y^+.

The ratios between two microscales $\tau_i^{\mathrm{L}}/\tau_i^{\mathrm{E}}$ are almost the same irrespective of the components. Those increase with y^+ and are approximated by Eq. (17).

The mean-square dispersion follows three stages as the dispersion time proceeds, i.e., Taylor's dispersion, shear effect stage and uniform dispersion stage, respectively. The mean-square dispersion in a short time range, of the order of T^{L}, follows usual Taylor's dispersion theory. In streamwise direction, due to the mean shear effect, t^3-dispersion appears after T_1^* that is a time scale of t^3-term evaluated from uniform shear dispersion theory by Riley and Corrsin (1974). The particle released from viscous sublayer follows t^n ($4 < n < 5$)-dispersion at $t > T_1^*$ but not t^3-dispersion because of strong inhomogeneity prevailing there. After the particles disperse uniformly between two walls, the streamwise dispersion is proportional to t^1 and the wall-normal dispersion is saturated to become constant. On the other hand, the spanwise dispersion follows the Taylor's dispersion because there is little influence of mean shear and wall constraints.

Acknowledgement

This research is supported by The Hori Information Science Promotion Foundation.

References

Bernard, P.S., Rovelstad, A.L., 1994. On the physical accuracy of scalar transport modeling in inhomogeneous turbulence. Phys. Fluids 6, 3093–3108.

Choi, J.-L., Yeo, K., Lee, C., 2004. Lagrangian statistics in turbulent channel flow. Phys. Fluids 16, 779–793.

Comte-Bellot, G., Corrsin, S., 1971. Simple Eulerian time correlation of full- and narrow-band velocity signals in grid-generated, 'isotropic' turbulence. J. Fluid Mech 48, 273.

Corrsin, S., 1953. Remarks on turbulent heat transfer. In: Proceeding of the Thermodynamics Symposium. University of Iowa, Iowa City, Iowa, pp. 5–30.

Deardorff, J.W., Peskin, R.L., 1970. Lagrangian statistics from numerically integrated turbulent channel flow. Phys. Fluids 13, 584–595.

Hanna, R.S., 1981. Lagrangian and Eulerian time-scale relations in the daytime boundary layer. J. Appl. Met. 20, 242–249.

Iida, O., Nagano, Y., 1998. The relaminarization mechanisms of turbulent channel flow at low Reynolds numbers. Flow Turbul. Combust. 60, 193–213.

Iliopoulos, I., Hanratty, T.J., 1999. Turbulent dispersion in a non-homogeneous field. J. Fluid Mech. 392, 45–71.

Kim, J., Hussain, F., 1993. Propagation velocity of perturbations in turbulent channel flow. Phys. Fluids A 5 (3), 695–706.

Koeltzsch, K., 1999. On the relationship between the Lagrangian and Eulerian time scale. Atmos. Env. 33, 117–128.

Kontomaris, K., Hanratty, T.J., Mclaughlin, J.B., 1992. An algorithm for tracking fluid particles in a spectral simulation of turbulent channel flow. J. Comput. Phys. 103, 231–242.

Legg, B.J., Raupach, M.R., 1982. Markov-chain simulations of particle dispersion in inhomogeneous flows: the drift velocity induced by a gradient in Eulerian ve- locity variance. Boundary Layer Met. 24, 3–13.

Mazumder, S., Modest, M.F., 1997. A stochastic Lagrangian model for near-wall turbulent heat transfer. J. Fluid Eng. 119, 46–52.

Mito, Y., Hanratty, T.J., 2002. Use of a modified Langevin equation to describe turbulent dispersion of fluid particles in a channel flow. Flow Turbul. Combust. 68, 1–26.

Nagano, Y., Tsuji, T., Houra, T., 1998. Structure of turbulent boundary layer subjected to adverse pressure gradient. Int. J. Heat Fluid Flow 19, 563–572.

Nishimura, F., 2000. Study of turbulence characteristics and large-scale streamwise vortical structure in a Couette flow. Doctor thesis, Nagoya Institute of Technology, Japan.

Pasquill, F., Smith, F.B., 1983. Atmospheric Diffusion. Halsted Press, New York.

Philip, J.R., 1967. Relation between Eulerian and Lagrangian statistics. Boundary Layer Turbulence (Physics of Fluids Supplement) 69.

Riley, J.J., Corrsin, S., 1974. The relation of turbulent diffusivities to Lagrangian velocity statistics for the simplest shear flow. J. Geophys. Res. 79, 1768–1771.

Sato, Y., Yamamoto, K., 1987. Lagrangian measurement of fluid particle motion in an isotropic turbulent field. J. Fluid Mech. 175, 183–199.

Schoppa, W., Hussain, F., 2000. Coherent structure dynamics in near-wall turbulence. Fluid Dyn. Res. 26, 119–139.

Shlien, D.J., Corrsin, S., 1974. A measurement of Lagrangian velocity autocorrelation in approximately isotropic turbulence. J. Fluid Mech. 62, 255–271.

Squires, K.D., Eaton, J.K., 1991. Lagrangian and Eulerian statistics obtained from direct numerical simulations of homogeneous turbulence. Phys. Fluids A 3, 130–143.

Taylor, G.I., 1921. Diffusion by continuous movements. Proc. London Math. Soc. 20, 196–211.

Taylor, G.I., 1953. Dispersion of solute matter in solvent flowing slowly through a tube. Proc. Roy. Soc. (London), Series A 219, 186–203.

Tennekes, H., Lumley, J.L., 1972. A First Course in Turbulence. MIT Press, 223-226.

Ushijima, T., Hu, Y., Kitoh, O., 2003. Numerical investigation of the relationship between Lagrangian and Eulerian statistics in a turbulent channel flow. In: Hanjalić, K., Nagano, Y., Tummers, M. (Eds.), Turbulence, Heat and Mass Transfer, vol. 4. Begell House, Inc., pp. 165–172.

Wang, Q., Squires, K.D., Wu, X., 1995. Lagrangian statistics in turbulent channel flow. Atmos. Env. 29, 2419–2427.

Yeung, P.K., Pope, S.B., 1989. Lagrangian statistics from direct numerical simulations of isotropic turbulence. J. Fluid Mech. 207, 531–586.